RADIATIVE TRANSFER IN GALAXIES

RADIATIVE TRANSFER IN GALAXIES

By
RORY WOODS, B.Sc., M.Sc.

A Thesis
Submitted to the School of Graduate Studies
in Partial Fulfillment of the Requirements
for the Degree of

Doctor of Philosophy

McMaster University

DOCTOR OF PHILOSOPHY (2015) McMaster University
(Physics and Astronomy) Hamilton, Ontario

TITLE: Radiative Transfer in Galaxy Formation

AUTHOR: Rory Woods, B.Sc. (Mount Allison University), M.Sc. (McMaster University)

SUPERVISOR: Professor James Wadsley

NUMBER OF PAGES: 1

Abstract

In this thesis, we present a novel algorithm for computing the radiation field in astrophysical simulations.

Dedicated to...

Acknowledgements

Thank you to all that helped.

"Some sort of quote?"

Albert Einstein (1879-1955)

Table of Contents

List of Figures

List of Tables

Chapter 1

Introduction

First part - what is this document? What will be in it? What is the main thing I will be telling you about?

1.1 Overview

Chapter 2 will go over the background of radiative transfer, etc.

Chapter 2

Radiative Transfer

This chapter will contain an overview of current radiative transfer methods and where we stand.

2.1 The Radiative Transfer Problem

$$j = \frac{dE}{dV d\Omega dt} \tag{2.1}$$

$$dI = jds \tag{2.2}$$

$$dI = -\alpha I ds = -n\sigma I ds = -\rho\kappa I ds \tag{2.3}$$

$$\frac{dI}{ds} = -\alpha I + j \tag{2.4}$$

$$I(s) = I(s_0) + \int_{s_0}^{s} j(s')ds' \tag{2.5}$$

$$I(s) = I(s_0) \exp\left[-\int_{s_0}^{s} \alpha(s')ds'\right] = I(s_0) \exp\left[-\tau(s)\right] \tag{2.6}$$

$$\tau(s) = \int_{s_0}^{s} \alpha(s')ds' = \int_{s_0}^{s} \rho(s')\kappa(s')ds' \tag{2.7}$$

2.2 Current Methods

The current set of computational methods can be classified as follows:

- Very accurate, expensive methods - monte carlo, ray tracing
- Methods accurate in specific scenarios, e.g. FLD for optically thick, "strömgren method" from Dale
- *Very* rough approximations, e.g. method that only looks at absorption near sink and source.

As will be seen, there is currently an opening in the market for something in the middle - Decent accuracy at a low cost.

2.2.1 Numerical Strategy for Solving RT

- RT is a function of seven variables - $x, y, z, \theta, \phi, t, \nu$.
- Simple division of each variable into 100 bins means storage of over 10^{14} elements, or roughly 1 Petabyte of data if each piece of information stored was ten bytes. First problem - large memory cost.
  - Note that 100 elements is minimal in many cases due to sharply peaked functions, e.g. ν.

  - 100x100 for angle only gives angular resolution of roughly 2.7° [not quite right - check this (steinacker 09 book)]

- RT equation is an integro-differential equation - difficult to use any sort of common solver.

Strategies include monte-carlo, ray tracing, grid-based solvers, and moment methods, each with certain advantages and disadvantages.

2.2.2 Monte-Carlo Solvers

In monte-carlo methods, a photon is carefully tracked through a domain, following scattering, absorption, and re-emission. See [from steinacker 09] **?????**). [ADD method basics]

- Advantages - can treat complicated spatial distributions, arbitrary scattering functions, and polarization.

- Disadvantages - Very high or low optical depths hard (why?), re-emission in all directions over many events hard (why?), no global error control

Chapter 3

The Numerical Method

In the absence of absorbing material, the problem of radiative transfer reduces down to that of gravity. As such, the tree-algorithm for calculating gravity can be used (**?**).

- A tree can be used to partition space.
- Each level of the tree holds finer partitions of the volume. See figure 3.1
- Each node of the tree contains accumulated information about the tree below it (total mass, etc.).
- In order to calculate gravity on a particular leaf (bucket), you can interact with the moment of another cell (3.1).
- To decide what level of the tree to interact with, you can define an opening angle/radius, θ. If a cell is smaller than this opening angle (the distribution of matter inside the cell is contained within a small enough angle on the sky), the entire cell can be used in the force calculation. If not, you must consider the child nodes separately. See equation 3.3.

- On average, the number of interactions a each particle will have is $\log N$, where N is the total number of particles. Thus, the force calculation for the whole simulation scales as $N \log N$. Note that lowering θ shifts the number of calculations that are approximated by large cells to smaller cells, and thus if θ is very small, the code approached scaling of order N^2.

- In the case of radiation, the math is very similar (See eq 3.2). However, since radiation does not cancel like forces, the dipole moment does not disappear and a rougher approximation is possible (wording wrong, fix this).

- In this case, the interaction scales as $N_{\rm sink} \log N_{\rm source}$. However, assuming the full tree is still used, the tree-build still scales as $N \log N$.

$$\Phi = \frac{G}{4\pi} \sum_{n=0}^{\infty} \frac{1}{r^{(n+1)}} \int (r')^n P_n(\cos\theta') \rho(\boldsymbol{r}') d\tau' \tag{3.1}$$

$$F = \frac{L}{4\pi r^2} \tag{3.2}$$

3.1 Tree Data Structures

In order to understand the radiative transfer algorithm that we are presenting, it is important to understand tree data structures.

- Terminology: Node, root node, leaf node, interior node, child, parent, sibling, tree build, walk the tree, ascend the tree, descend the tree.

- In computer science, a tree is a hierarchical data structure. Typically the tree starts at a single point, usually called the root node, and branches out to many other "child" nodes.

- Each node in the tree stores some sort of data, and the relative location of the node in the tree indicates the relation of the data in the node to the data in other nodes.

- GASOLINE uses a "k-d tree" for gravity. This is an example of a binary space-partitioning tree. Every node contains 2 children, and each node of the tree represents a particular volume of space. kd-Trees and octrees represent the majority of trees used in astrophysical simulations. See figure 3.1 for visual examples of trees.

3.2 Building a Radiation Tree

- While the algorithm we present is general enough to work with any volume-filling tree, the following sections will introduce the algorithm as we have developed it. GASOLINE uses a k-d tree for its gravity solver, and as such, our version of the algorithm uses this tree type in order to make use of existing tools in the code base.

- The recursive pseudocode for the tree-build is presented below (note - change to nice pseudocode format):

    1. if number of data elements greater than n_{leaf}, partition data
    2. recursively call build tree on each partition of the data set

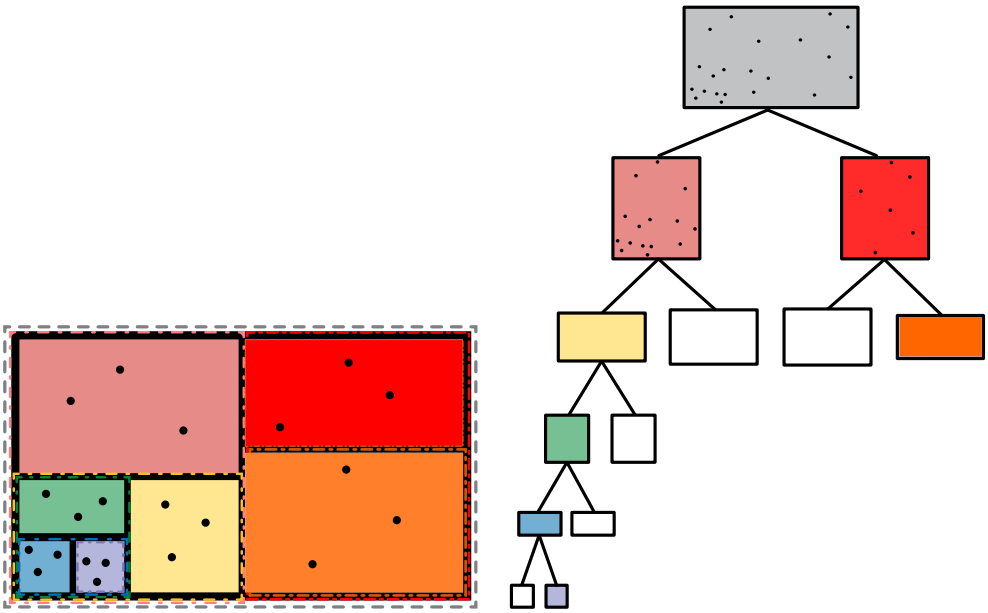

Figure 3.1: This is an example of a binary tree. The volume is represented by a tree node, and each volume is then split into two subvolumes, which are represented by two "child" nodes of the original node. This splitting can continue indefinitely on either side, making the tree an effective way at splitting volumes.

3. else, if number of data elements less than n_{leaf}, calculate basic cell properties

4. After if statement, calculate accumulated cell properties (higher moments, etc)

- In our case, the partition data step involves finding the longest axis of the data contained on the current node and dividing particles to the upper and lower halves of the midway point of that axis.

- Each volume and its corresponding list of particles is then passed recursively to the tree build function again. This terminates when build tree receives a list of particles that is sufficiently short (less than a user set

parameter, n_{leaf}). At this point, basic cell properties such as center of luminosity and total luminosity are calculated.

- Once the leaf nodes have been calculated, more complicated average properties, such as higher moments, can be calculated by looping through all particles in the node. This applies to both leaf and interior nodes.

- The initial partition function does not require that the data be fully sorted, only that it be divided to either side of an intermediate value. This is an order n operation.

- The tree will be roughly of depth $\log(N)$, meaning that the partition will need to be performed $\log N$ times. Therefore, the tree build should scale as roughly $N \log N$.

- For radiation, average cell properties that are used are average density, average opacity, standard deviation of opacity, total luminosity, and center of luminosity.

- Note that we have calculated center of luminosity without taking into account absorption within the cell.

3.3 Exchanging Radiation

Once the tree has been built, calculating the radiation (gravity) at any particular point can be accomplished by traversing the tree structure, a process called a "tree walk."

- First, a "post-order" tree walk is performed in which the children of a node are always checked before its sibling. The walk continues until it

arrives at a leaf node, at which point the radiation (gravity) arriving at that leaf is calculated. This leaf node will be called the receiving leaf.

- The second walk occurs during the radiation (gravity) calculation. We must check what cells are acceptable to interact with based on the opening angle criteria mentioned in the chapter 3 introduction. We can make use of the fact that no children below a cell that has already accepted the θ criterion need be checked, as they are contained within the cell and so automatically satisfy the criteria of their parent.

- The algorithm looks like:

    1. Given a cell (starting with the root cell), check if the distance, r, from the current leaf to the cell is shorter than the opening radius (given by equation 3.4).

    2. If r is shorter than the opening radius, the cell must be "opened," meaning that we return to step 1, but now passing in each child node to check.

    3. If r is longer than the opening radius, the cell is acceptable to interact with. The radiation may be calculated to the bucket using equation 3.5. See figure 3.2.

    4. In the case that the distance to the cell is smaller than the opening radius, and the node has no children (e.g. for leaves of the tree that are very spatially close to the receiving leaf), the interaction should not be approximated, and the direct n^2 summation over all particles in each leaf is performed.

5. Once radiation has been calculated from the current cell, the tree-walk is allowed to skip all children of the current cell and move on to its sibling or parent's sibling (parent's sibling in the case that we are the right-hand child of the parent node).

- Once radiation has been calculated for the receiving bucket, we move on to the next bucket, which is accomplished by moving to the sibling if the current bucket is the left child of the parent node, or to the sibling of the parent node if we are the right child. An example radiation exchange is shown in figure 3.3.

- The above algorithm will run in $N \log N$ time, as with gravity. However, unlike gravity, not all objects emit radiation. Thus, technically the more specific scaling is $N_{\rm sink} \log N_{\rm source}$. The slow growth rate of computation time with the number of sources makes the algorithm a very strong candidate for cosmological applications in which there are often similar numbers of star particles to gas particles. In fact, some codes have already made use of this basic idea (**???**). As well, the algorithm may allow for the treatment of gas particles as sources (more caerful considerations must be made to tie the radiation to the cooling of the gas in this case), which is rarely done due to incredibly high computational cost.

$$\theta_{\rm crit} = \frac{b_{\rm max}}{r} \tag{3.3}$$

$$r_{\rm crit} = \frac{b_{\rm max}}{\theta_{\rm crit}} \tag{3.4}$$

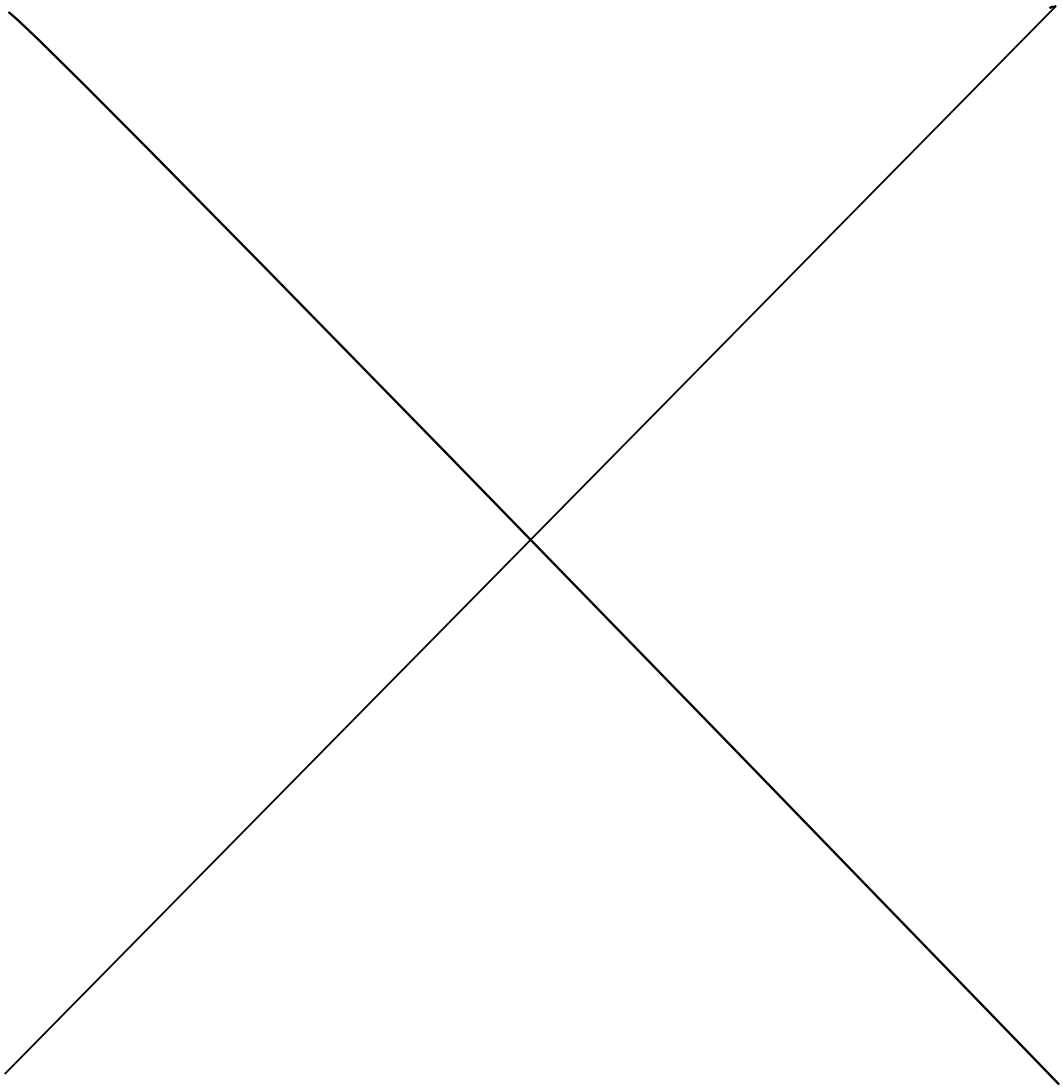

Figure 3.2: Cell A in this image is the receiving cell, while cells B, C, and D are cells that A will receive flux from. Cell A is close enough so that it should be opened, but is a leaf and so it requires a direct n^2 summation. Cell C is close enough and is not a leaf, so it will have its two children checked for the same criteria (the left child will be too close, the right child will be acceptable to interact with). Cell D is not a leaf, but is sufficiently far away that leaf A can interact with the full cell.

$$F_{\text{bucket}} = \frac{L_{\text{tot}}}{4\pi r^2} e^{-\tau} \tag{3.5}$$

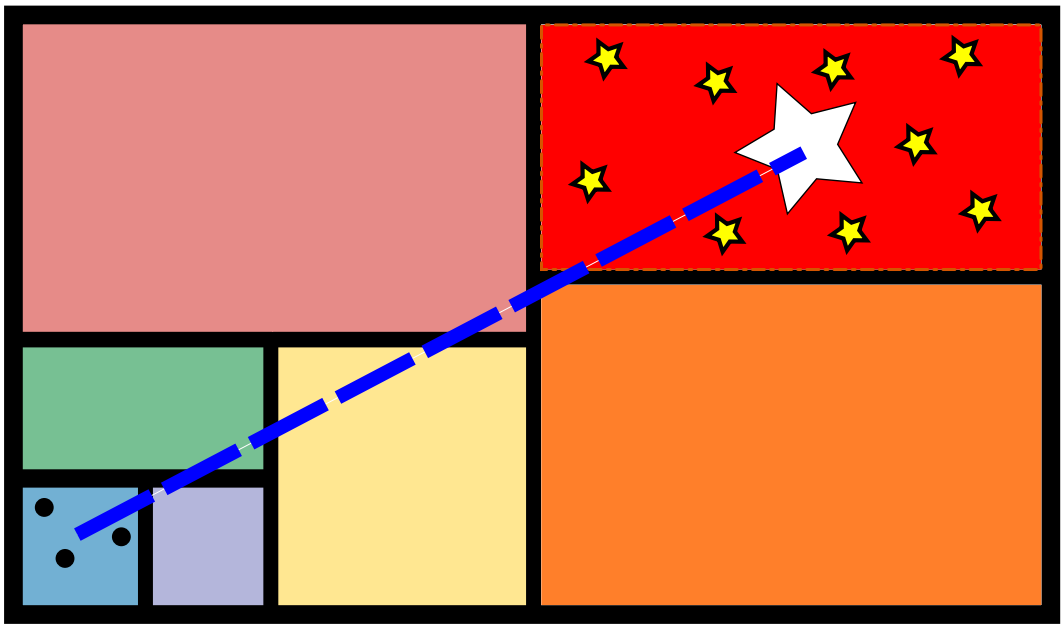

Figure 3.3: In this image, cell A is receiving radiation from cell B. Cell B is sufficiently far away that we can find the center of luminosities of all the sources inside of it, and calculate flux based on that single value rather than summing each one individually.

3.4 Absorption

The algorithm presented in sections 3.2 and 3.3 assumes that no change to the radiation (force) happens in between the sending and receiving buckets. In gravity, this is acceptable because forces are not "absorbed" in any way. However, radiation tends to be absorbed and scattered by intervening material and thus the intensity of the radiation at a point is not only due to the sending source, but to all material in between the source and the sink.

- As mentioned in chapter 1, most current radiative transfer codes either completely ignore intervening material or do very detailed tracing of photons throughout the medium. The former option produces very bad radiation fields while the latter is incredibly computationally expensive.

- In order to reproduce the behavior of equation 2.4, we must modify the algorithm to be able to find the optical depth between any two points. However, we must be careful not to lose the performance afforded by the tree. In order to do this, we have developed the algorithm to make use of the tree during the optical depth calculation as well.

- The crucial point to the algorithm lies in the fact that for any two interacting cells, there exists a common parent node. Thus, all intervening space between the cells must lie within the subtree in which the common parent is the root.

- If we traverse up the depth of the tree (hereafter referred to as a tree climb) once from each interacting node to the common parent node, we will have performed roughly $\log(N)$ extra operations per interaction. If we do no other work than this, then our scaling for radiative transfer changes to $N_{\rm sink} \log N_{\rm source} \log N$. While the extra factor of $\log N$ is certainly worth noting, it does not tend to increase scaling by a significant amount.

- Our goal then becomes to perform order (1) amount of work during this additional tree climb.

- In order to accomplish this, we need only make use of the average properties recorded for each cell during the tree build.

- At each higher cell during the tree climb, we obtain a larger representative volume from that cell. The new volume contains the previous volume as well as a new contribution from the previous cell's sibling. This sibling's volume may or may not lie on the vector connecting the

two interacting cells. This can be determined by calculating the distance to the edge of the current volume along the vector from the centers of the original interacting cells. This operation is completed in order (1) time. (introduce this algorithm?).

- At each new higher cell, if the calculated line segment is longer than the accumulated distance so far, than the difference is the amount of the vector contained in the additional volume. By recording this new line segment, the average density of the cell, and the average opacity of the cell (both values that were accumulated during the tree build), then we have everything needed to calculate the optical depth of the line segment according to equation 2.7. By summing the optical depth of each line segment, we will have obtained the full optical depth between the interacting cells in order $logN$ time. The algorithm is depicted graphically in figure 3.4

3.5 Refinement

While section 3.4 introduces a very fast algorithm for calculating a radiation field, it relies heavily on the geometry of the underlying tree. In volumes with very smooth density/opacity, the above algorithm performs very well. However, in cases with sharp density/opacity gradients, the density/opacity gradient is discretized into widths of order the cell size at the current tree depth. This can become problematic, causing the tree structure to be imposed into the calculated radiation field. In order to solve this, we introduce a refinement process to the algorithm that allows a descent back down the tree

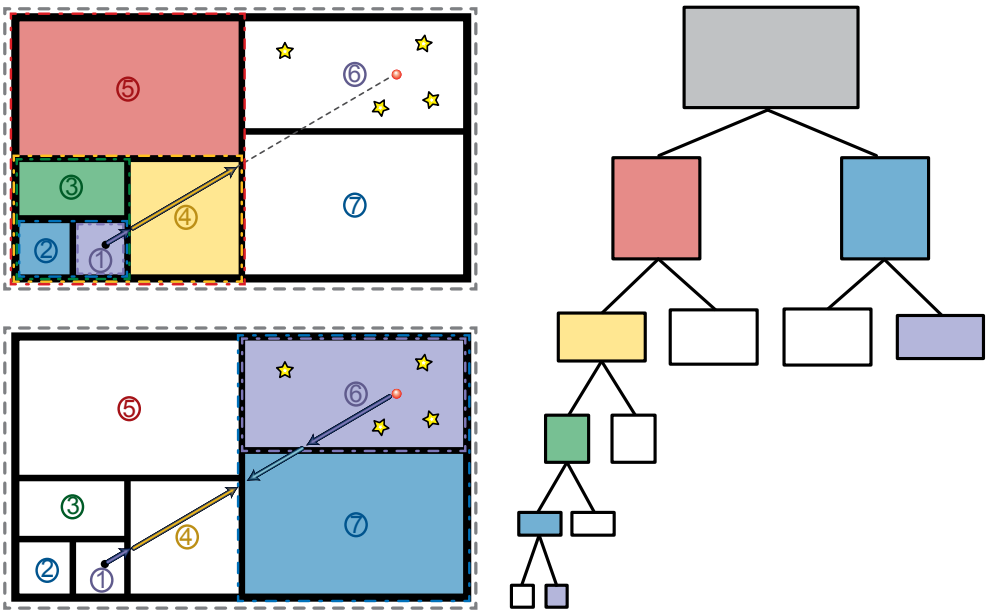

(a) A representation of the algorithm in real space, with the tree overlaid.

(b) The colors correspond to the volumes on the left.

Figure 3.4: The absorption algorithm.

during the tree climb in order to obtain a more detailed description of the medium.

- The refinement is a fairly straightforward addition to the algorithm. At the point where the average properties of the cell would normally be considered, we simply check if the current cell passes a refinement criteria.

- If the cell passes the criteria to refine, rather than recording the average properties, we recursively check the children of section of the tree we did *not* ascend from.

- Once we arrive at a cell that fails the criteria to refine (or at a leaf and can no longer refine), we record the line segment within the cell and the average properties as normal, and return up the recursive call. See figure

3.5 for a visual representation.

- The specific refinement criteria has deliberately been left vague until this point. In principle, one can refine on any cell property desired.
- For the purposes of this paper, we have decided to use an opacity refinement criteria. Within any cell, if a constant times the standard deviation of the average opacity is larger than the average opacity, the cell is refined. We find this produces a reasonable amount of refinement in code tests.
- Note that this is not necessarily the ideal criteria for physical simulations. It would be wise not only to look at the variation in opacity, but also the absolute value. In cases where the optical depth is very high, most of the radiation will be absorbed anyway, and the algorithm can be terminated since this particular vector yields a negligible flux of photons to the receiving cell.

Extension of the refinement to ray-tracing

- If very high accuracy is required, the refinement routine is flexible enough that sub-leaf refinement is possible. While this has not currently been tested since it leaves the regime of low computational expense, it could easily be implemented.
- If a leaf was reached during refinement and still passed the criteria to be refined on, the individual particles inside the cell could be considered.
- A ray tracing scheme through the cell similar to SPHRay (**?**) could be performed. The machinery to do this ray trace is already established for use within the receiving and sending cells (see section 3.6 and figure 3.6).

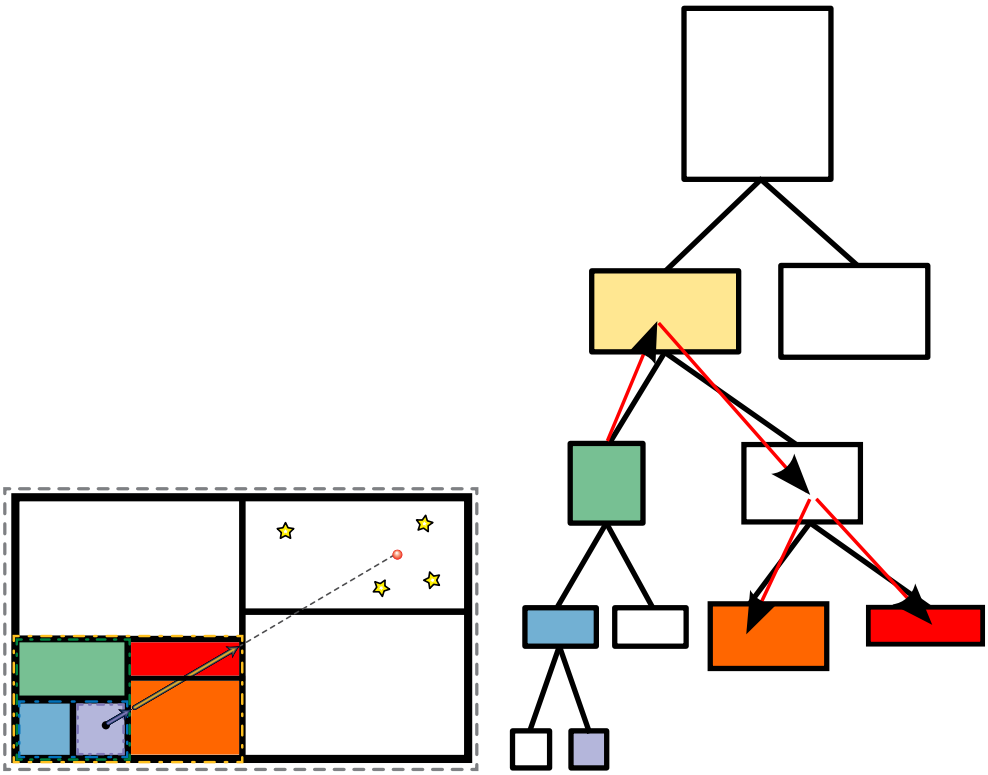

(a) The tree splits the line segment into the red and orange sections.

(b) The colors correspond to the volumes on the left.

Figure 3.5: When the line segment is too rough in some physical sense, refinement can be triggered. Visually, the algorithm descends back down the tree the opposite direction it came from until the criteria to refine is no longer satisfied or until a leaf is reached.

3.6 Resolving the Receiving Cells

During testing, we ran into issues with ionization fronts "stalling" in certain cells. If a sharp ionization front is passing through a receiving bucket, then the effects of averaging can cause issues if the optical depth of the bucket is of order unity or higher. (below section needs re-wording and more specifics).

- Consider an ionization front that has passed halfway through a leaf node (half of the particles are ionizaed, half are not).

- The average opacity will be $\kappa/2$, where κ is the opacity of the unionized particles.
- The ionized particles will use an opacity that is much too large, therefore reducing the flux that particles at the "rear" of the leaf see.
- This means that particles at the rear of the leaf are harder to ionize than at the front, and the propagation speed of the front is drastically reduced.
- In order to combat this, more detailed tracing is required *only in the receiving leaf.*
- This is easily accomplished by implementing a scheme similar to SPHRay (**?**). (introduce simpler method that we use where we order particles along vector and linearly add optical depth?). See figure 3.6.

Introducing the ray tracing machinery for the above purpose also creates the ability to ray trace within leaves during the refine mentioned in section 3.5. In principle, this means the code can easily be forced into a full ray trace if this behavior is desired.

3.6.1 High Optical Depth Particles

High tau particles are problematic. This is how we deal with them...

3.7 Periodicity

Move to future work?

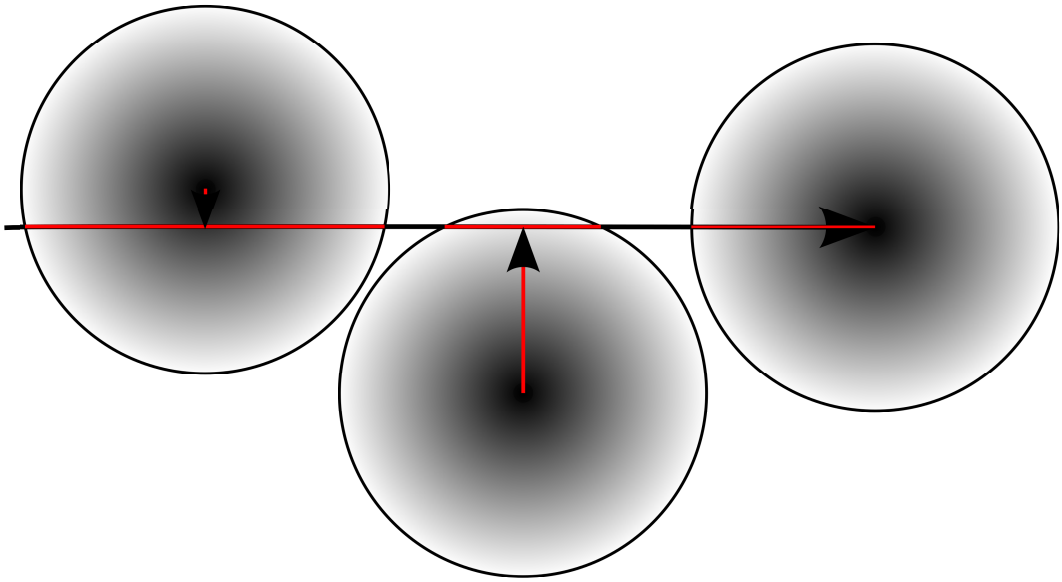

Figure 3.6: Two ray tracing schemes. The first is the scheme of **?**) in which the photons are diminished by optical depth along each particle's smoothing length that they pass through. The second scheme is much simpler and yields very similar results. It relies on the fact that the ray actually represents a very large cone of photons, and that most particles in the cell will probably contribute to the absorption of photons at the receiving particle. It essentially simplifies to setting b = 0 for every particle in the receiving leaf.

3.8 Cosmological Background Radiation

In order to do cosmological simulations properly, we must account for the radiation coming from the rest of the universe outside of the simulation volume. Most current codes apply a constant UV field to the entire box, essentially the lowest order approximation possible.

- Few codes have moved past this for cosmology, though some have.
- OTVET (**?**) uses their radiation scheme with periodic boundaries.
- Other more detailed scheme apply a constant radiation field at the boundaries coming into the volume (add citations).

- While our scheme is perfectly capable of doing a periodic option, we have opted to set up a number of "background sources." The sources are distributed on the surface of a sphere at the very edge of the simulation (or larger if required) and the number of sources can be varied to match the required angular resolution of the background.

- Finding the flux at the center of a sphere of sources is a problem akin to Newton's Shell Theorem. However, because the flux doesn't cancel like force, the solution does not work out the same. See equation 3.6.

- Since the solution is logarithmic in r, the we can assume the flux is roughly constant at similar radii. Since most cosmological zoom simulations only consider gas at a fairly small radius, this is acceptable.

$$F = K\left[\log R + r - ln(R - r)\right] \tag{3.6}$$

3.9 Cosmological Effects

Move this section to "future plans" section?

3.9.1 Cosmological Redshift of Radiation

3.9.2 Accounting for a Finite Speed of Light

Move this section to "'future plans" section?

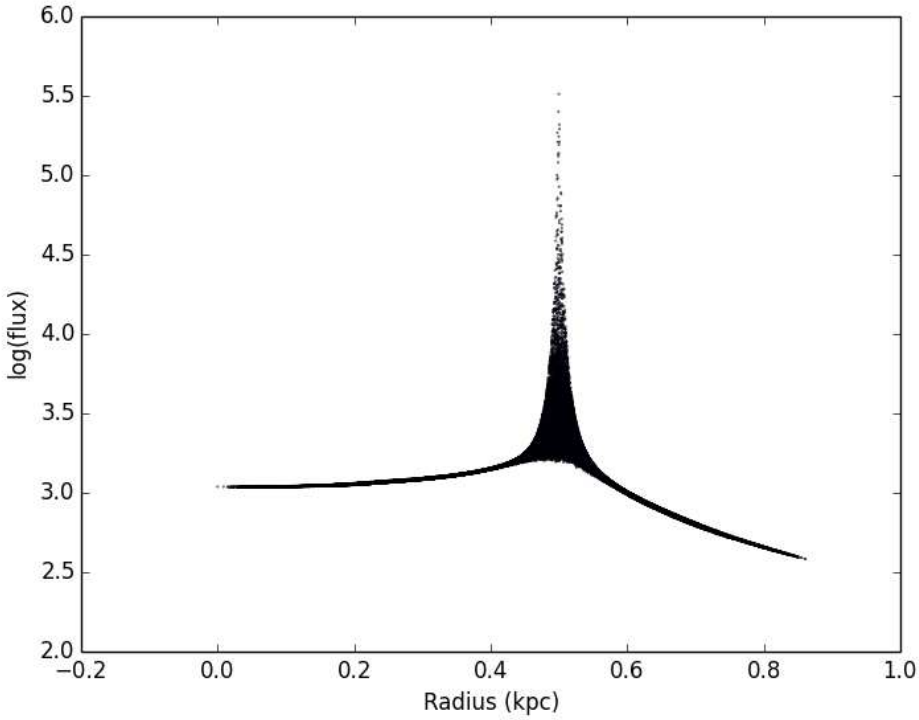

Figure 3.7: The distribution of flux particles receive due to cosmological background particles when distributed in a sphere at the edge of the box. Note that value of the flux at the center can be easily scaled by simply scaling the luminosity of all sources on the sphere.

3.10 Summary of Algorithm

We have presented a flexible and computationally inexpensive algorithm for calculating the radiation field within a simulation. The algorithm affords many benefits (note: need to introduce many of stated benefits below in previous sections):

- It is flexible enough to allow a wide range of accuracy depending on the application. Speed starts at $N \log N \log N$ and approaches that of ray tracing (check this...) when the algorithm is tuned to that level of refinement.

- Because radiation is transferred instantaneously, the speed of light does not become a limiting time step. If ionization dynamics are important, then the propagation of the ionization front becomes the limiting time step. If only end behavior is required, then the there is very little the algorithm does to limit the time step.

- There is no scan dependence. Because flux is accumulated at each receiving bucket without explicitly depositing the photons into the intervening material, ionization/heating/cooling is performed completely separate to radiation. This means that the solution will not change based on the order in which the sources are visited.

- The algorithm is independent of wavelength or even number of wavelengths. The algorithm need only perform the tree walk and tree climb a single time in order to obtain the line segments in each cell. Performing different wavebands simply equates to recording multiple average opacities. This enables multi-band radiative transfer at little additional cost.

However, it is important to keep in mind the limitations and assumptions of this algorithm.

- Photons are not explicitly conserved. In order to save computational time, we can not keep track of the photons deposited in intervening material during an exchange. We obtain an optical depth and simply assume that the photons lost in the process have been deposited in the intervening material. When the intervening material is the receiving bucket at a later point in the algorithm, it should receive roughly the correct number of photons due to a matching initial segment (wording...).

- Light is transferred instantaneously, meaning that photon fronts could travel faster than allowed, and that sinks could receive photons from a source too far away to have sent photons there yet.

- Very large opacities in single particles can be problematic for both cooling (calculating the emitted flux from a particle is complex if the particle itself is optically thick) and ionization propagation. Particle self-absorption can impart the same "stall" in a single particle that was mentioned in section 3.6 for leaves.

- Extra computation time can be required in the heating and cooling code due to intense local radiation fields. However, if the goal is to obtain a radiation field, this is already a built in cost to any algorithm. We simply mention it to suggest that increased computation time is due not only to the radiation algorithm, but the increased computation time for the cooling integrations (remove this point?).

Chapter 4

Code Tests

In this chapter, I present a variety of tests to demonstrate the strengths and limitations of the above algorithm. Many tests cases have been drawn from previous RT papers including **???**). This chapter also include tests of accuracy and scaling of the algorithm.

4.1 Glass

A glass of particles is a simple way to demonstrate the most basic functionality of the algorithm. Each particle effectively acts to sample the radiation field at a particular point and has an easily calculated exact solution to compare to. A glass is also the relaxed state for an SPH simulation

4.1.1 Optically Thin

TAKE THIS SECTION OUT? TOO SIMPLE?

In the optically thin case, we simply want to ensure that we obtain a $1/r^2$ dropoff with flux. There should be no errors present in this test case

because in the case of a single source, no averaging is needed and both exact luminosity and position of the source is used for every sink.

$$F = \frac{L}{4\pi r^2} \tag{4.1}$$

4.1.2 Optically Thick

TAKE THIS SECTION OUT? TOO SIMPLE?

Like section 4.1.1, this section aims to demonstrate the base ability of the code. In this case, the glass of particles has a roughly homogeneous density and thus the flux is still easily calculated for comparison.

- The equation for flux in this case is still fairly simple. If we refer to equation 2.6, we can see the theoretical flux is simply equation 4.1 multiplied by the exponential of optical depth. See equation 4.2.
- This assumes a homogeneous density field. The glass does not have an exactly homogeneous field, but has little variance from the average.
- Figure 4.1 shows the error distribution of the particles.
- Note that in the case that the density field is exact, the errors reduce down to machine precision. This emphasizes the importance of accurately modeling the density distribution.

$$F = \frac{L}{4\pi r^2} \exp -\tau \tag{4.2}$$

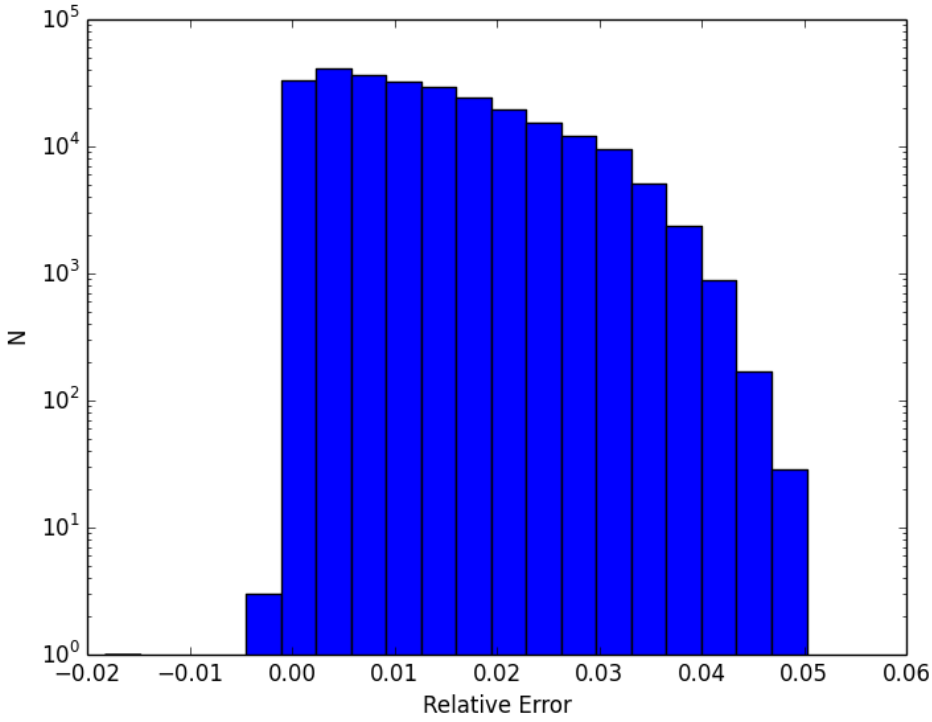

Figure 4.1: The distribution of flux errors among particles.

4.2 Multi-Source Glass

We now show the effect of including many sources. The code is now performing at its most "stressed;" having a large number of randomly distributed sources means the code will run at its slowest and will include a large amount of averaging (not quite right).

- We first present the optically thin case. In this case, the glass has had half of its gas particles replaced with sources so that there are an equal number of each.
- The error distribution present in this

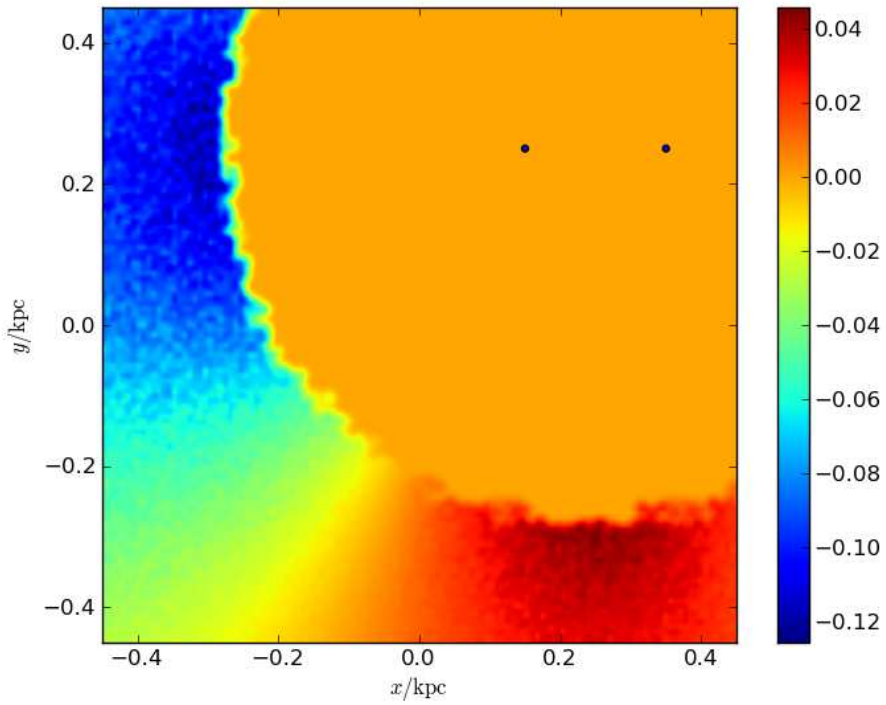

Figure 4.2: The error associated with averaging star positions.

4.3 Effects of Averaging the Source

We now look closely at what effects averaging sources can have on results.

4.3.1 Two star

4.3.2 Isothermal Sphere with a Cluster(?)

Words

4.4 The Strömgren Sphere

The strömgren sphere is a theoretical ionized sphere of gas. It was first discussed by Bengt Strömgren in 1938 (**?**). We start with a cloud of homogeneous neutral Hydrogen gas and an ionizing source, commonly representing an O or B-type star, at the center. As the photons from the source ionize the hydrogen, the optical depth of the gas decreases, and so the ionizing photons move further out creating an ionization front. As the front moves out, the photon density as a function of radius falls off simply due to $1/r^2$ geometry and eventually a point is reached where the ionization rate falls to the recombination rate. At this point, the front stops in equilibrium.

One can solve for this radius by setting the photon density as a function of radius to the recombination rate and solving for radius (**??**),

$$R_S = \left(\frac{3}{4\pi} \frac{\dot{N}_\gamma}{\alpha n_H^2} \right). \tag{4.3}$$

One can also find the growth rate of the front,

$$R(t) = R_S[1 - \exp\left(t/t_{\text{recomb}}\right)]^{1/3}. \tag{4.4}$$

The above equations are the solutions for the evolution of a sharp ionization front, meaning that we have assumed the transition from ionized to neutral is infinitesimal in size. In order to solve for a non-sharp front, we must solve some equations numerically. FILL IN METHOD HERE.

4.4.1 The Isothermal Case

In the simplest case, the ionizing source is assumed to emit photons at exactly 13.7 ev, meaning that the hydrogen gas is ionized but not heated. Cooling is also disabled, meaning that the gas is isothermal. If we assume that the ionization front propagates until the ionization rate drops low enough (due to geometric diminishment) to equal the recombination rate of the ambient medium, then we can solve for the equilibrium ionization radius by setting the two rates equal.

The ionization rate per unit volume can be written as the (fill in here)

$$R_S = \left(\frac{3}{4\pi} \frac{\dot{N}_\gamma}{\alpha n_H^2} \right) \tag{4.5}$$

$$R(t) = R_S[1 - \exp\left(t/t_{\rm recomb}\right)]^{1/3} \tag{4.6}$$

The above derivation assumes a "sharp" ionization front, meaning the transition from ionized to neutral is across an infinitesimal region. In practice, the transition region is small compared to the size of the ionized region, but there is structure interior to the Strömgren radius that is not accounted for by simply solving for the equilibrium radius. In order to solve for a non-sharp ionization front, we must integrate the above ionization equations (**?**). (ADD HERE). In the following tests, we include both the sharp and non-sharp ionization front solutions for comparison to our results.

We follow the initial conditions of **?**); the medium is initially neutral with a temperature 1e5 K and a density of 1e-3 $\rm cm^{-3}$. An ionizing source is turned on at t = 0 that emits $\dot{N} = 5e48$ photons $\rm s^{-1}$ at 13.6 ev. We use a cross

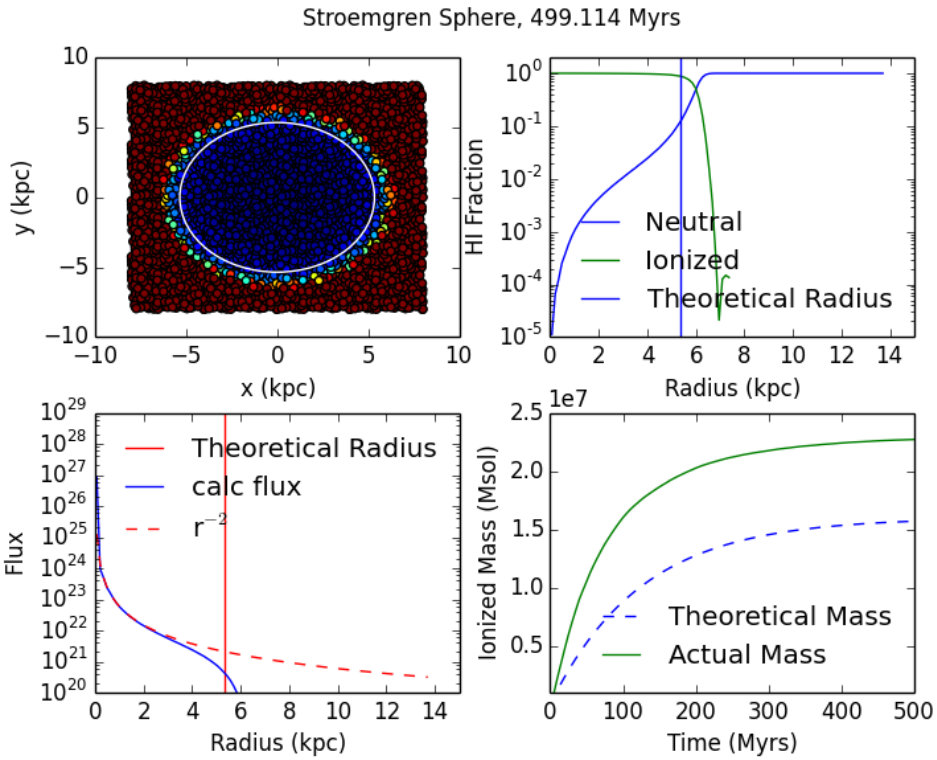

Figure 4.3: A slice of particles showing the ionization state.

section $\sigma = 6.3e-18cm^2$ and a recombination rate of $\alpha = 2.59e-13cm^{-3}s^{-1}$, typical of 1e5 K gas. These values give a Strömgren radius of 5.38 kpc and a recombination time of 125 Myr.

4.4.2 The Thermal Case

The above formulation assumed the gas was isothermal and that all incident photons had the same energy. In reality, photons range across many wavelengths (commonly in a Planck spectrum) with differing cross sections for each wavelength. As well, absorption typically causes heating, which effects, among many properties, recombination rate.

In order to do a more realistic test,the incident photons are assumed to

be from a black body with temperature 1e5 K. The cross section is changed to an integrated cross section, obtained by integrating the cross section as a function of wavelength over all wavelengths having energies between 13.6 ev and 29.65 ev. The gas has an initial temperature, This scenario does not have an analytic solution to compare to, and so we instead compare to the results of ?) and ?). (NOTE - seems to be inconsistency. 10^5 K source corresponds to 43 ev = 29.65 + 13.6, but other areas seem to indicate total energy of 29.65, not heating energy = 29.65. Figure this out).

This test includes heating due to absorption and cooling due to recombination Λ_r, collisional ionization Λ_{ci}, line cooling Λ_l, and Bremsstrahlung radiation Λ_B. The rate are taken from ?) in order to match ?). The following are those rates in ergs cm^{-3} s^{-1}:

$$\Lambda_r = 8.7 \times 10^{-27} \sqrt{T} \left(\frac{T}{10^3 K}\right)^{-0.2} \Bigg/ \left[1 + \left(\frac{T}{10^6 K}\right)^{0.7}\right], \tag{4.7}$$

$$\Lambda_{ci} = 1.27 \times 10^{21} \sqrt{T} \left(1 + \sqrt{\frac{T}{10^5 K}}\right) e^{157809.1/T} n_e n_{HII}, \tag{4.8}$$

$$\Lambda_l = 7.5 \times 10^{-19} \left(1 + \sqrt{\frac{T}{10^5 K}}\right)^{-1} e^{-118348/T} n_e n_{HI}, \tag{4.9}$$

$$\Lambda_B = 1.42 \times 10^{-27} g_{ff} \sqrt{T} n_e, \tag{4.10}$$

where $g_{ff} = 1.3$ is the gaunt factor.

Figure 4.4 shows a radially averaged profile of temperature. We see a peak temperature of roughly $3 \times 10^4 K$ with a radial dropoff stimilar to results from ?). This demonstrates the code's ability to couple radiation to the thermodynamics of the gas (ADD MORE).

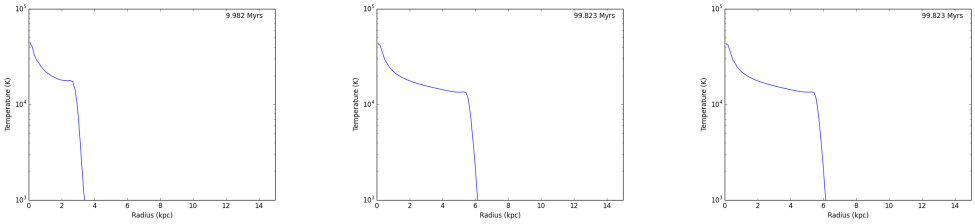

Figure 4.4: Temperature vs radius for the thermal Strömgren sphere.

4.5 The Gas Wall

In order to test the algorithm's ability to handle a sharp density jump, we again perform the isothermal stromgren front (section 4.4.1), but with a large density jump. We keep all of the same initial parameters, but change the density to the left of x = 0 to $\rho/2$ and the density to the right of x = 0 to $3/2\rho$.

4.5.1 Only Radiation

In the case that hydrodynamics is off, the solution is two strömgren hemispheres centered at x = 0.

4.5.2 With Hydrodynamics - the Champagne Flow

In order to test the coupling of radiation to the hydrodynamics, we perform a similar test in which the code now uses its hydrodynamics solvers. We follow the setup of **?**); A 50 pc cube is initialized with a density of 0.055 atoms cm^{-3} to the right of x = 0, and 63 atoms cm^3 to the left. The temperatures of the left and right halves are 55 K and 6.3e3 K, respectively. This density/temperature combination gives pressure equilibrium at the boundary. An ionizing source

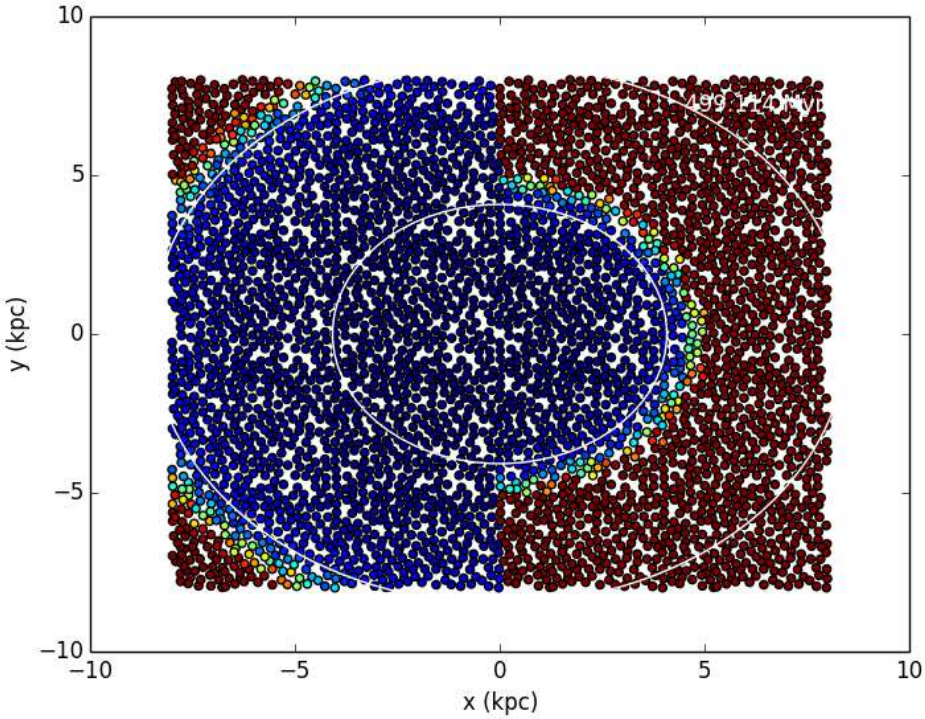

Figure 4.5: Two slabs of gas at different densities.

is turned on at the origin that emits 5.3e47 photons/s, similar to a type BO.5 star. The combination of density and luminosity gives a stromgren sphere radius of 1.5 pc in the dense regio ns and a recombination time of 2.48e4 Years. The simulation is run for more than 4e6 years, meaning that the gas has time to heat and expand.

4.6 Shadowing

Text to fix the formatting.

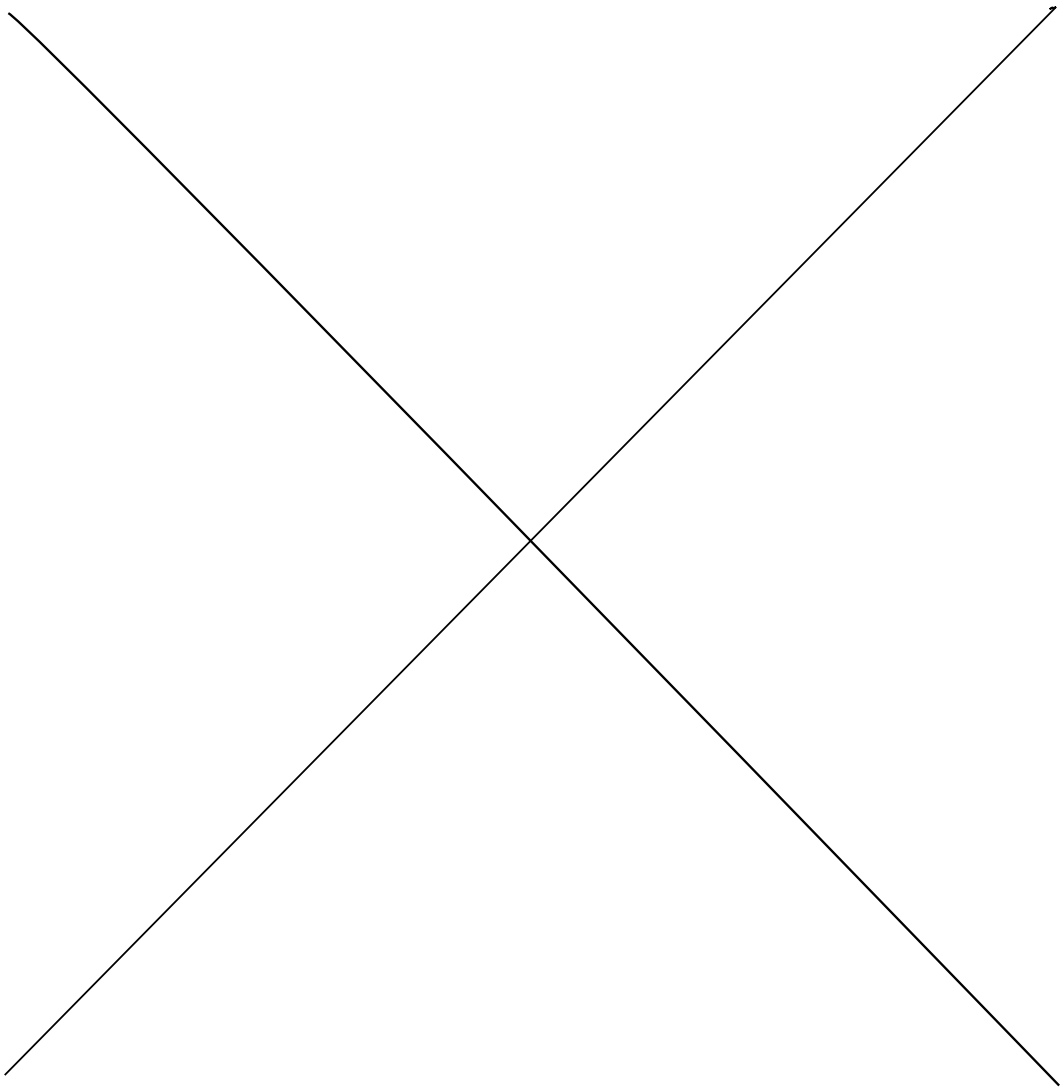

Figure 4.6: An example of a champagne flow.

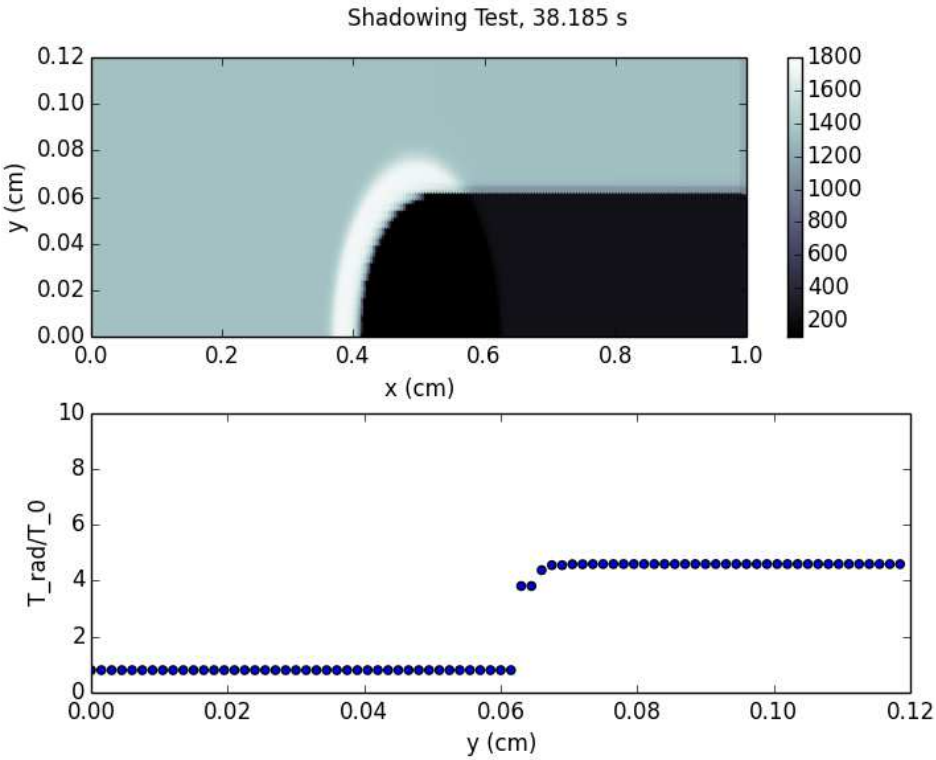

Figure 4.7: Demonstrating the codes ability to shadow.

4.7 Galaxy Disk

Text to fix the formatting.

4.8 Timings and Scaling

Text to fix the formatting.

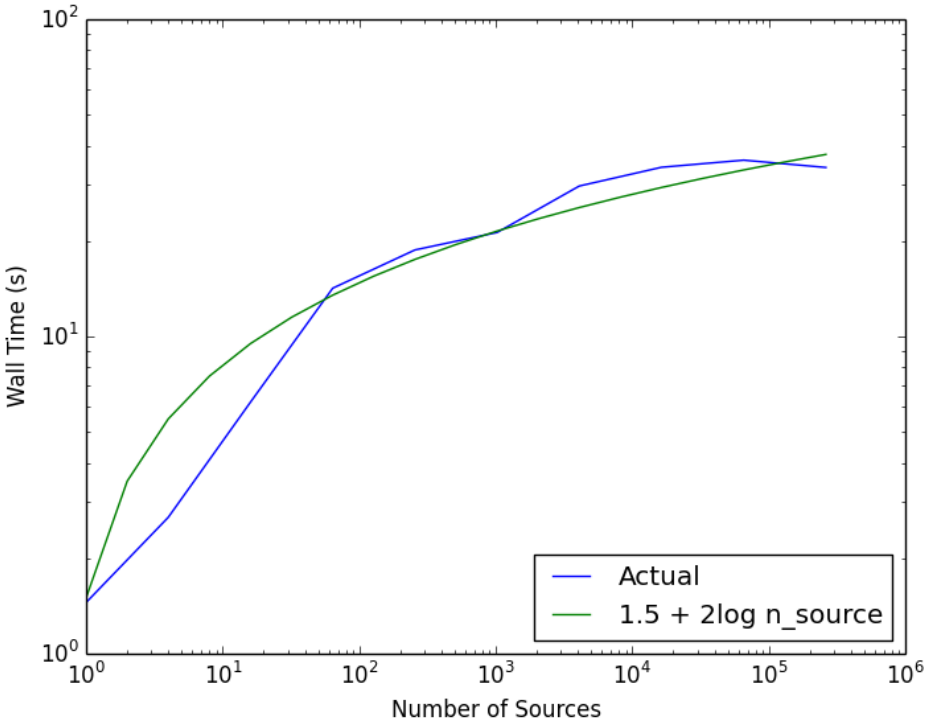

Figure 4.8: Wall time vs the number of sources.

Chapter 5

Applications to Galaxy Formation (Future Work?)

In this chapter, we discuss current and planned applications of the algorithm.

5.1 Galactic UV Fields

Currently, there is very little work in computational astrophysics that models the UV fields in and around galaxies. While many models have been created from the observational side [references], due to large computational cost, simulations have left this area largely unexplored or explored only at high redshift [references].

We have used [will be using] the above algorithm to re-run the MUGS2 comparison project [cite Ben].

- What effect does radiation have on the galaxy in MUGS2 (as a function of redshift, all the way to redshift 0)?
  - What effect does UV have on the ISM? (sam?)

  - What effect does UV have on satellite galaxies, gas properties, SFR - shut down mechanism?
  - What is the typical escape fraction of UV in galaxies (isolated disk from Sam, consistent with results from MUGS? Compare to Kannan et al. escape fractions)
  - Compare to observations of UV fields

Future work of this algorithm is quite broad; the flexibility allows application to a wide range of problems. The following are immediately planned projects, and following that is a short list of unplanned but possibly interesting projects.

- Look at H2 formation and destruction using Ly-Werner bands of radiation (Charlotte). How does cloud shielding depend on density? Compare to OWLS/EAGLE w/ TRAPHIC (Rahmati+ 13ab) (this is HI shielding and ntot H2 shielding... not great comparison?).
- Considering the properties of the ISM and molecular clouds (Samantha, Sijing). [Author] suggests 4 radiation bands are needed to sufficiently find ISM properties. Using these 4 bands, calculate effect of radiation on ISM. How do gas properties effect SFR and vice versa? [ask Sam for more info here]
- Potential to look at the effect of radiation processing. How does processing radiation (UV re-emitted as IR) effect the gas properties? How important of an effect is it in determining SFR? This project depends on a successful implementation of a self consistent gas source function. Can we do this in a stable way with respect to the cooling code?

- An obvious application is cosmic re-ionization, but this has already been done a bit since it does not require running to low redshift. That said, can we do it better/cheaper? Do our results agree?

Chapter 6

Conclusions and Future Work

Appendix A

Appendix A